Wavelength Tunable Single Nanowire Lasers Based on Surface Plasmon Polariton Enhanced Burstein–Moss Effect

ARTICLE *in* NANO LETTERS · OCTOBER 2013

Impact Factor: 13.59 · DOI: 10.1021/nl402836x · Source: PubMed

5 AUTHORS, INCLUDING:

Qihua Xiong
Nanyang Technological University
166 PUBLICATIONS **3,978** CITATIONS

SEE PROFILE

Tze Chien Sum
Nanyang Technological University
142 PUBLICATIONS **3,501** CITATIONS

SEE PROFILE

NANO LETTERS

Letter

pubs.acs.org/NanoLett

Wavelength Tunable Single Nanowire Lasers Based on Surface Plasmon Polariton Enhanced Burstein–Moss Effect

Xinfeng Liu,[†,∥] Qing Zhang,[†,∥] Jing Ngei Yip,[†] Qihua Xiong,*[,†,‡] and Tze Chien Sum*[,†,§]

[†]Division of Physics and Applied Physics, School of Physical and Mathematical Sciences, Nanyang Technological University, Singapore 637371

[‡]NOVITAS, Nanoelectronics Center of Excellence, School of Electrical and Electronic Engineering, Nanyang Technological University, Singapore 639798

[§]Energy Research Institute @ NTU (ERI@N), Nanyang Technological University, 50 Nanyang Drive, Singapore 637553

Supporting Information

ABSTRACT: Wavelength tunable semiconductor nanowire (NW) lasers are promising for multifunctional applications ranging from optical communication to spectroscopy analysis. Here, we present a demonstration of utilizing the surface plasmon polariton (SPP) enhanced Burstein–Moss (BM) effect to tune the lasing wavelength of a single semiconductor NW. The photonic lasing mode of the CdS NW (with length ~10 μm and diameter ~220 nm) significantly blue shifts from 504 to 483 nm at room temperature when the NW is in close proximity to the Au film. Systematic steady state power dependent photoluminescence (PL) and time-resolved PL studies validate that the BM effect in the hybrid CdS NW devices is greatly enhanced as a consequence of the strong coupling between the SPP and CdS excitons. With decreasing dielectric layer thickness h from 100 to 5 nm, the enhancement of the BM effect becomes stronger, leading to a larger blue shift of the lasing wavelength. Measurements of enhanced exciton emission intensities and recombination rates in the presence of Au film further support the strong interaction between SPP and excitons, which is consistent with the simulation results.

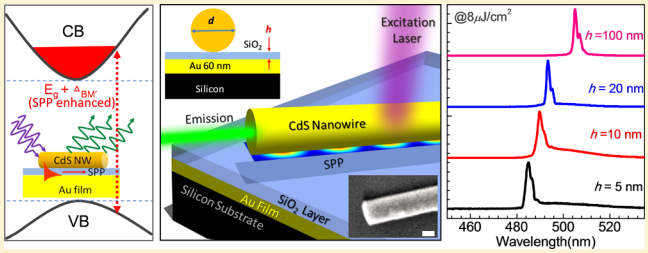

KEYWORDS: *Nanowire laser, tunable wavelength, Burstein–Moss effect, surface plasmon polariton, CdS nanowires, ultrafast optical spectroscopy*

Semiconductor nanowires (NWs) present a unique system for exploring physical phenomena at the nanoscale and are also expected to play a critical role in future electronic and optoelectronic devices.[1−3] They have garnered even more attention because of recent demonstrations in all-optical active switching,[4] hot carrier luminescence,[5] semiconductor NW based solar cells,[6] and electrically/optically pumped NW lasers.[7−9] For the application as NW lasers, the ability to tune the lasing wavelength is of utmost importance for wavelength variable applications such as optical communications, sensing, signal processing, spectroscopy analysis, and so forth.[10−12] Tunable semiconductor NW and nanoribbon lasers have been realized by simply tuning the nanostructure bandgap with composition tunable gain media.[13,14] Through controlled synthesis of multiquantum-well core/shell NW heterostructures, Qian et al. demonstrated wavelength tunable GaN NW lasers.[15] Recently, a simple approach to tune the laser wavelengths of a single undoped semiconductor NW based on the intrinsic self-absorption of the gain media was also reported.[7,16]

Parallel to these exciting developments, surface plasmons have also been subjected to intense scrutiny because they can offer unique approaches to manipulate the optical energy in the subwavelength regime.[17,18] A surface plasmon polariton (SPP) is a transverse magnetic (TM)-polarized optical surface wave that propagates along a metal–dielectric interface, typically at visible or infrared wavelengths.[19] A variety of fascinating phenomena, including enhanced fluorescence and Raman scattering of single molecules,[20,21] enhanced nonlinear effects,[22,23] extraordinary transmission through subwavelength hole arrays,[24] and SPP amplifiers and lasers,[25,26] have been demonstrated utilizing the strong confinement properties of the SPP. More recently, it was also demonstrated that enhanced light-matter interaction occurs for molecules placed inside a nanometer scale gap of a plasmonic waveguide with enhancements to the spontaneous emission rate up to ~60 times due to the strong optical localization in two dimensions.[27] Even larger enhancement of the spontaneous emission by ~1000 times was reported for the case where a fluorescence dye was placed between the gap of a silver film and a silver NW.[28] Nonetheless, works on integrating these two fields and synergistically leveraging on their unique properties for SPP-enhanced

Received: July 29, 2013
Revised: September 23, 2013
Published: October 17, 2013

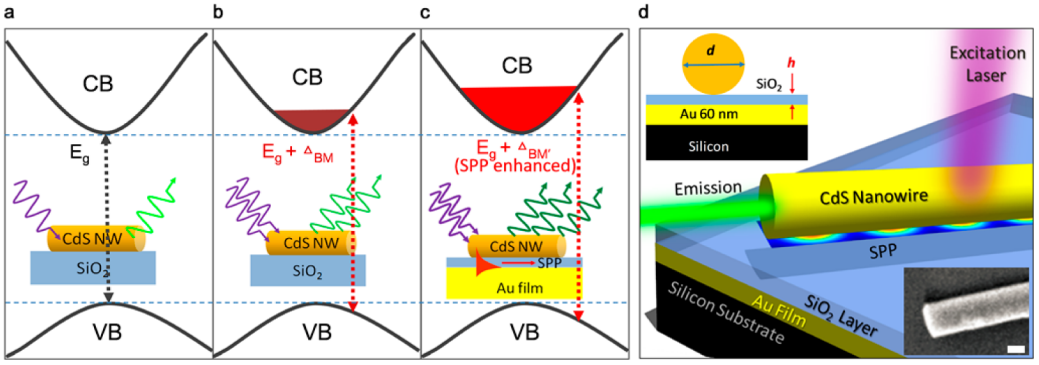

Figure 1. An illustration of the various effects on the band gap energy of nondoped semiconductor NWs: (a) without the BM effect (under low pump fluence), (b) with the BM effect (under high pump fluence), and (c) the SPP enhanced BM effect, where Δ_{BM} is the BM shift and Δ_{BM}' is the SPP enhanced BM shift. (d) A schematic of the NW laser devices; the CdS NW on top of the Au film (60 nm) is separated by a nanometer scale SiO_2 buffer layer of thickness h nm. The diameter of the CdS NW is d nm. Inset (bottom right corner) is the SEM image of a typical single CdS NW on top of a gold film with h = 5 nm and the scale bar is 100 nm.

tunability of the NW lasing wavelengths remain largely unexplored.

The Burstein–Moss (BM) effect is the apparent blue shift of the optical gap of a semiconductor as a consequence of state-filling close to its conduction band (see Figure 1a,b).[29,30] The magnitude of the BM shift (Δ_{BM}) from free-electron theory is proportional to $n_e^{2/3}$, where n_e is the electron carrier concentration.[31,32] Potentially, the BM shift could be used to tailor the spectral shift and gain from the NW cavity, thereby achieving laser wavelength tunability.[33] However, it is extremely challenging to obtain large spectral shifts from undoped semiconductor NWs, given that its BM effect is very weak.[7,34] One exciting possibility to overcome this weak BM effect would be to utilize the SPPs to modulate the carrier concentrations in the semiconductor bands through energy transfer (see Figure 1c), thus enhancing the BM effect. Demonstrating lasing wavelength tunability in single NWs through the SPP-enhanced BM effect is the main focus of this work. This approach possesses significant potential for further development to achieve active modulation of the NW lasing wavelengths.

Herein, we demonstrate that the lasing wavelength of a single CdS NW laser significantly blue shifts more than 20 nm at room temperature through the SPP-enhanced BM effect. Systematic steady state power dependent photoluminescence (PL) and time-resolved PL (TRPL) studies validate that the BM effect in the CdS NW is strongly enhanced in the hybrid metal/dielectric/semiconductor structures due to the strong coupling between the CdS excitons and SPP. Further attestation of this finding is from the measurements of enhanced exciton emission intensities and rates in the sample with the thinnest dielectric layer. Such manipulation of hybrid-plasmon-polariton holds great promise for the next generation on-chip circuits integrated with photonic and plasmonic laser source.[35,36]

A schematic of our designed NW laser device is shown in Figure 1d, comprising of the following components: a single CdS NW (of diameter d) is placed on a nanometer-scale SiO_2 layer (of thickness h) overcoating an Au film with a thickness of ~60 nm. Evidence of the high CdS NW crystalline quality is provided in the Supporting Information (Figure S1). A semiconductor/dielectric/metal design was selected over a metal-semiconductor design because of lower losses in the former, which is essential for the clear demonstration of this phenomenon. Furthermore, this latter configuration offers ultrasmall volume confinement over a broad range of frequencies that is ideal for wavelength tunability. The CdS NWs were fabricated using a vapor transport method found in previous literature.[37,38] The Au film and SiO_2 layer were prepared by thermal evaporation.[39,40] Figure 1d inset shows a scanning electron microscopy (SEM) micrograph of a typical CdS NW with diameter of ~220 nm.

The optical measurements were performed using a home-built confocal microscope system equipped with the following excitation sources: a 76 MHz Ti:Sapphire oscillator and a 1 kHz Ti:Sapphire regenerative amplifier (see Supporting Information Figure S2). The steady-state band-edge emission (BE) from the CdS NW was collected using in a conventional backscattering geometry dispersed by a grating of 300 g/mm and detected by a thermoelectric-cooled charge coupled detector (CCD) camera. TRPL data were collected using a streak camera system equipped with temporal scan units operating at the above repetition rates. These hybrid NW laser devices were optically pumped with 400 nm laser pulses that were frequency doubled from the fundamental 800 nm of these lasers using a beta barium borate (BBO) crystal.

Figure 2a–d shows the emission spectra of four CdS NW devices with different thickness of h (5, 10, 20, 100 nm). The excitation pump fluence increases from 0.1 to 8 $\mu J/cm^2$. Given that the CdS NW lasing wavelength is dependent on the NW dimensions (i.e., diameter and length, see Supporting Information Figure S3), extreme care was taken to select a series of CdS NWs with approximately the same length (i.e., ~10 ± 0.5 μm) and diameter (i.e., ~220 ± 10 nm) to eliminate any size-dependent effects. The transition from spontaneous emission to lasing action can be observed for the four CdS NW devices; Supporting Information Figure S4 shows a representative NW device illustrating the process. The lasing threshold for CdS NWs on SiO_2 of thickness h = 5, 10, 20 nm is between 2 and 3 $\mu J/cm^2$, which is comparable to the threshold value of ~2 $\mu J/cm^2$ at h = 100 nm. The comparable lasing threshold of these CdS NWs further validates that the lasing originates from the photonic modes rather than the plasmonic modes. Plasmonic lasing occurs at a much higher threshold which will be discussed later.[41] To make a clear comparison of the lasing wavelengths of the four devices, the four lasing spectra with a fixed pump fluence of 8 $\mu J/cm^2$ were plotted in Figure 2e. It can be seen that the lasing wavelength is tuned from 504 nm (h = 100 nm) to 483 nm (h = 5 nm). A series of CdS NW

dx.doi.org/10.1021/nl402836x | Nano Lett. 2013, 13, 5336–5343

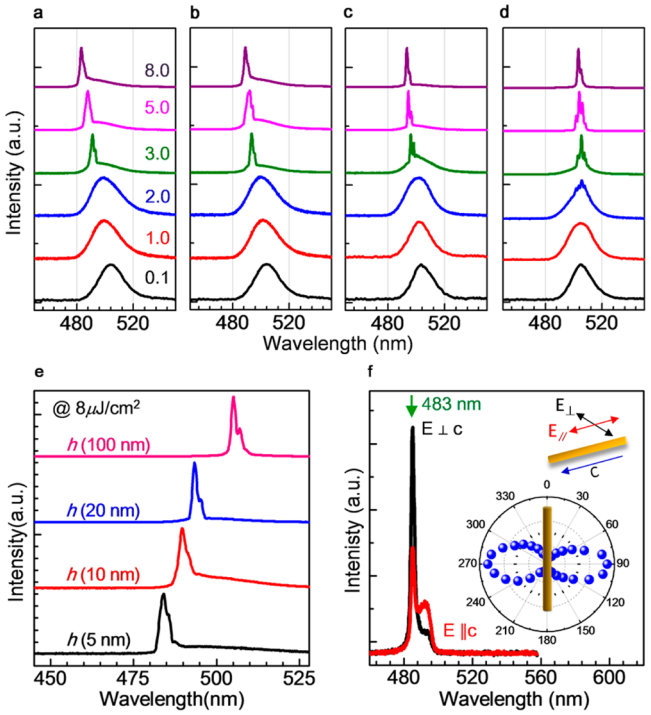

Figure 2. The emission spectra of four CdS NW devices with excitation pump fluence increasing from 0.1 to 8 μJ/cm^2; these four CdS NWs have almost the same length (~10 μm) and diameter (~220 nm); on substrates with different thickness of SiO_2, (a) h = 5 nm, (b) h = 10 nm (c) h = 20 nm, (d) h = 100 nm. (e) The lasing peaks of four devices under the same pump fluence of 8 μJ/cm^2. (f) Polarization-dependent experiments: polarization-sensitive lasing spectra for a CdS NW with buffer layer h = 5 nm with the polarization oriented parallel (red curve) and perpendicular (black curve) to the NW long axis (i.e., c-axis is along the NW length). Inset is a polar plot of the lasing emission intensity at ~483 nm.

devices on substrates with different h were measured at the pump fluence of 8 μJ/cm^2 and similar trends are obtained, as shown in Supporting Information Figure S5. Compared with previously reported tuning methods, this tuning range of >20 nm is considerable for undoped CdS NW.[11,42] Exciton-SPP coupling in the hybrid devices with thinner SiO_2 layers is strongly suspected and we seek to ascertain its presence in the subsequent paragraphs. Nonetheless, the nature of this lasing behavior in all cases was verified to be photonic rather than plasmonic in origin. Figure 2f shows that the polarization of the emission from the hybrid device with h = 5 nm is perpendicular to the axis of the NW.[41] SPP, which are TM waves at the metal−dielectric interface, on the other hand would yield emissions whose polarization is parallel to the NW long axis.[11,43] The influence of the pump laser's polarization to these results could be discounted as a quarter waveplate was used to change the initial linear pump polarization to circular polarization for the photoexcitation. Previously, a similar structure was used to realize plasmonic nanolasers.[11,41] In those reports, a silver film was used as the SPP media because of its minimal plasmonic damping in the visible and near-IR range. Their main purpose was to form an ideal plasmonic nanocavity between the silver film and the semiconductor nanowire/nanorod with the latter functioning as the gain medium, leading to the realization of SPP oscillators, known as SPP lasers or "spasers".[19] However, for our case only the photonic lasing mode is observed because of the following two reasons: (i) Au has an interband transition in visible range,[43] therefore the propagating distance of the plasmonic modes would be short, making it hard to support the plasmonic lasing modes; and (ii) the diameter of the NWs is relatively large (220 nm), permitting the photonic modes to exist inside the NW.

Prior to establishing the presence of any exciton-SPP coupling in these hybrid devices, it is essential that we first gain a clear understanding of the pump-power dependent spectral shift of the bare CdS NWs and its mechanism (in the absence of any coupling). Extensive pump fluence dependence studies on CdS NWs with different diameters (i.e., ~100, ~200, and ~300 nm) were performed to scrutinize the characteristic blue shift of the emission peak energy with increasing pump laser power from 0.1 to 2 μJ/cm^2.[33,44] At low pump fluence (0.1 μJ/cm^2), the BE peaks of the 100, 200, and 300 nm CdS

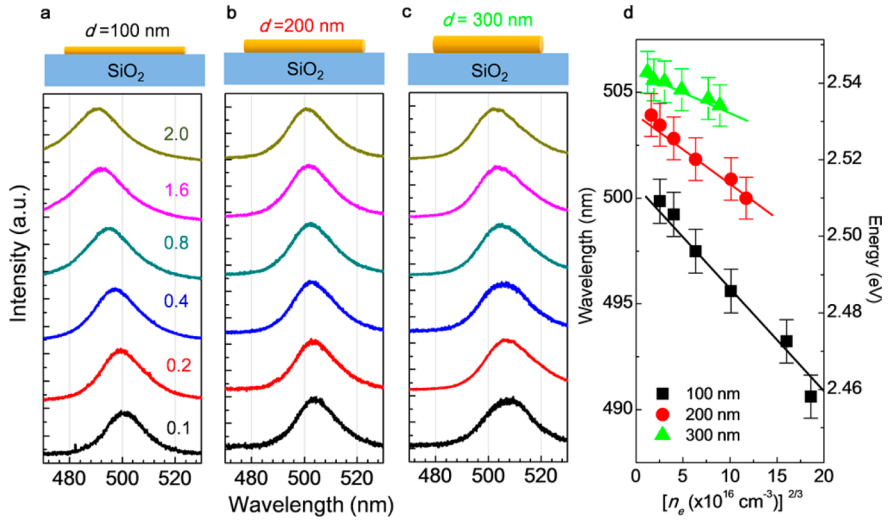

Figure 3. Power-dependent PL spectra of CdS NWs on SiO_2 substrates with diameters of (a) ~100, (b) ~200, and (c) ~300 nm with pump fluence increasing from 0.1 to 2 μJ/cm^2. The 400 nm laser pump pulses was frequency doubled from the Mira oscillator. (d) The emission peak wavelength versus the electron carrier density $n_e^{2/3}$, the linear fit (according to eq 1) suggests that the blue shift of the peak wavelength is attributed to the BM effects.

dx.doi.org/10.1021/nl402836x | Nano Lett. 2013, 13, 5336−5343

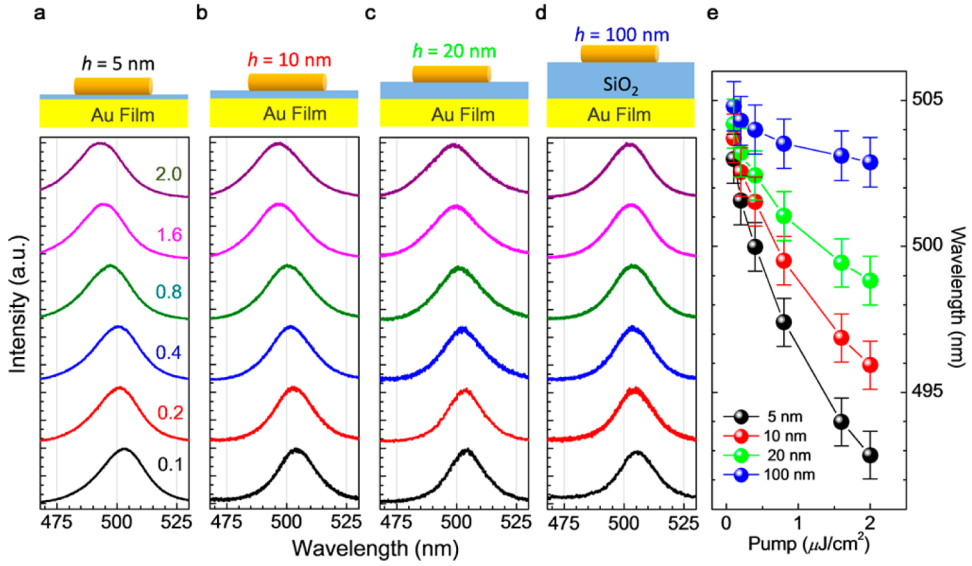

Figure 4. PL spectra of individual CdS NWs (length ~10 μm and diameter ~220 nm) on Au films with different SiO_2 buffer layer thickness (h) as a function of pump power from 0.1 to 2 $\mu J/cm^2$ for h = (a) 5, (b) 10, (c) 20, and (d) 100 nm, plotted for comparison. (e) The emission peak positions of the four NWs shown in (a–d) with increasing pump power from 0.1 to 2 $\mu J/cm^2$. The lines are guides for the eye.

NW are 500, 504, and 506 nm, respectively. The slight difference in peak wavelengths of CdS NWs with different diameters is attributed to the surface depletion induced quantum confinement effect (see Supporting Information Figure S3).[39] With increasing pump power up to 2 $\mu J/cm^2$, a pronounced blue shift of the emission peak can be observed in these three samples, as shown in Figure 3a–c.

Among the above diameters, the 100 nm CdS NW, which has the most evident signature of this phenomenon, was selected as the reference sample to elucidate the mechanism of the spectral blue shift and emission broadening. The pump power dependence of the peak wavelength for the 100 nm CdS NW is summarized in Figure 3d. The magnitude of the shifts is quantified by fits to a Gaussian using a Levenberg–Marquardt nonlinear least-squares algorithm. Over the range of the pump power investigated, blue shift of ~10 nm (~51 meV) are observed. Such spectral blue shift has previously been reported in CdS quantum dots and NWs[43–46] and could arise from a few origins: (1) the Burstein–Moss (BM) effect due to the excess conduction band electrons;[29,30] (2) an increase in excitonic energy due to excess surface-trapped electrons;[47,48] (3) a decrease in the oscillator strength of the excitonic transitions due to trapped electrons and holes;[46,49] and (4) Columbic screening by photogenerated free carriers.[31,50] Mechanisms (2) and (3) could be ruled out as these would be more dominant for small semiconductor clusters/NWs with very large surface to volume ratios (e.g., in the case where the diameter of particle/NW is comparable to the Bohr radius of CdS excitons ~3 nm). Mechanism (4) could also be ruled out because the blue shift ~51 meV (see Figure 3d) observed for CdS NW is much larger than that caused by the screening effect (i.e., equals to the ionization energy of excitons ~28 meV).[51] Hence, we can attribute the spectral blue shift to the BM effect. These results collectively verify that the BM shift is indeed relatively weak in the undoped CdS NWs (and without any SPP coupling).

The magnitude of the BM shift can be expressed as

$$\Delta_{BM} = \frac{\hbar^2}{2m^*}(3\pi^2 n_e)^{2/3} \quad (1)$$

where m^* is the reduced effective mass and is derived from the valence and conduction band effective masses, m_v^* and m_c^*, according to $1/m^* = 1/m_v^* + 1/m_c^*$. n_e is the electron concentration, expressed as $n_e = F/(\hbar\omega_0 d)$, where $\hbar\omega_0$ is the photon energy and d is diameter of the NW; F is the pump fluence (in J/m^2 per pulse).[52] Since the pulse width of laser (150 fs) is much shorter than the exciton decay constant, exciton diffusion need not be considered. To determine n_e, the amount of light absorption from a single NW is needed. Unlike its thin film counterpart, the strong scattering from the NW precludes the use of the Lambert–Beer's law.[53] Instead, an estimate was performed using the measured scattering and transmission spectrum of a single NW. Assuming that each photon generates an electron–hole pair, our calculations show that ~57% of the incident photons are absorbed by the 100 nm diameter CdS NW (Supporting Information, Figure S6). Hence, at a threshold fluence of ~2 $\mu J/cm^2$, n_e ~6.0×10^{17} cm^{-3}, which is comparable to the critical Mott transition density (~6.5×10^{17} cm^{-3}) and sufficient for the BM effect to occur. Using eq 1, a good fit of the pump power dependent BM shift is evidently shown in Figure 3d. It suggests that the BM effect clearly captures the essential physics of these phenomena in these NWs.

Next, we turn our attention to examine the exciton-SPP interaction in these hybrid devices and their influence on the BM effect. We compare the magnitude of the blue shift of the PL spectra for CdS NWs (length ~10 μm and diameter ~220 nm) on substrates with different SiO_2 thickness h (top of Figure 4a–d). For the device with h = 100 nm, only ~2 nm PL peak shift with increasing pump power suggests the absence of strong interaction between the CdS excitons and the SPPs. With decreasing SiO_2 layer thickness between the CdS NW and Au film, a more pronounced blue shift is observed. With increasing pump power from 0.1 to 2 $\mu J/cm^2$, a blue shift of ~11, ~7, and ~5 nm were obtained for h = 5, 10, and 20 nm, respectively. A summary of the CdS NW emission peak

dx.doi.org/10.1021/nl402836x | Nano Lett. 2013, 13, 5336–5343

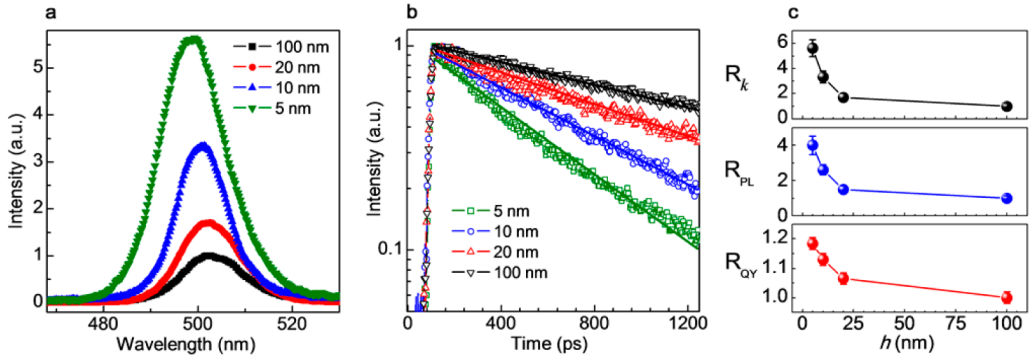

Figure 5. (a) The steady state PL spectra of the four NWs at a pump power of 1.0 μJ/cm^2, these spectra are normalized using the reference sample with h = 100 nm. (b) The corresponding (normalized) PL decay transients from the PL spectra are shown in panel a. (c) Thickness-dependent decay rate enhancement R_k, PL intensity enhancement R_{PL}, and the quantum yield enhancement R_{QY} factors. The lines are guides for the eye. The h = 100 nm sample is used as the reference.

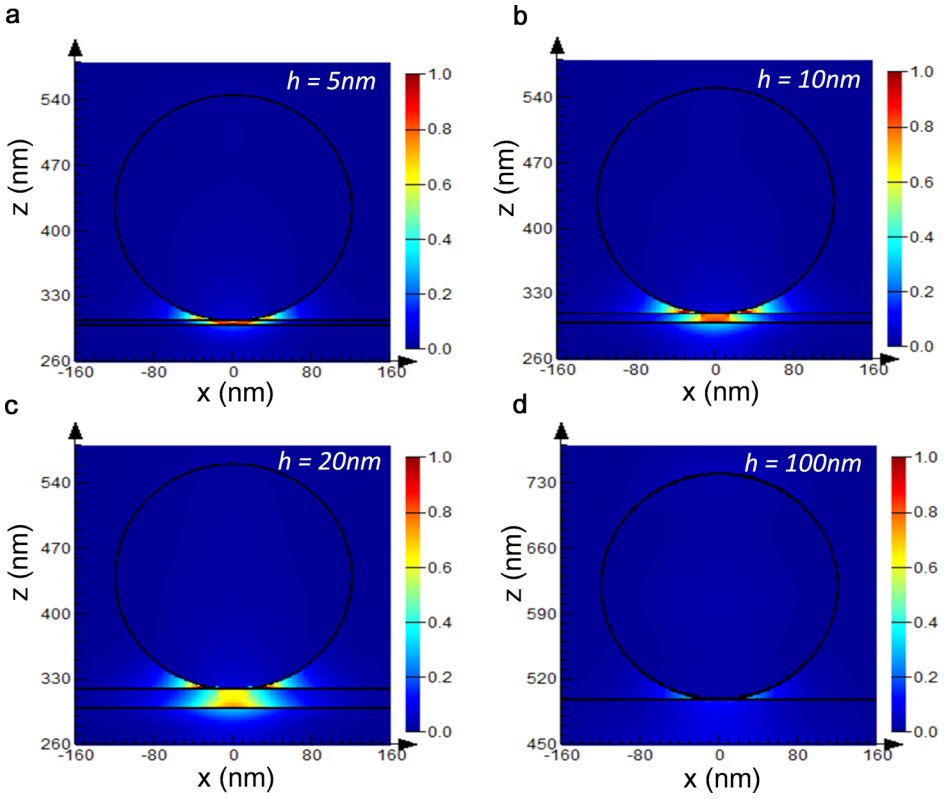

Figure 6. FDTD simulations of the electric field distribution in the x−z plane between the CdS NW (with diameter of ∼220 nm) and Au film (thickness of ∼60 nm), with different SiO_2 gaps (a) h = 5 nm, (b) h = 10 nm, (c) h = 20 nm, and (d) h = 100 nm. The color maps represent the $|E(x, z)|$ of the hybrid plasmonic mode at a wavelength of ∼495 nm. The black circles represent the profiles of the CdS NW and the two horizontal black lines are the profiles of the SiO_2 layer.

position as a function of pump power is given in Figure 4e. The increasing blue shift with decreasing layer thickness indicates that the interaction between the local surface plasmon field in the Au film and the CdS NW play an important role in enhancing the BM effect. These layer thickness dependent blue-shifts of the emission peaks follow the same trend as that of the lasing wavelengths as shown in Figure 2a. It should be noted that the lasing wavelength in nanowire cavities are mainly determined by the following two factors: (i) the gain wavelength region within the spontaneous emission profile; and (ii) the NW cavity described by the Fabry−Perot modes.[45,46] The SPP-exciton coupling would affect the PL emission profile and inevitably the lasing wavelength. Therefore, the significant blue shifts of both the emission peak energy and lasing wavelengths provide compelling evidence of an SPP enhanced BM effect in these hybrid CdS/SiO_2/Au devices.

To obtain further validation of the SPP enhanced BM effect, the PL intensities and the exciton recombination rates were monitored as the coupling between the SPP and excitons were modulated. Figure 5a shows the PL spectra of the four CdS NW samples. The spectra intensities are normalized to that of the h = 100 nm sample. The strongest PL enhancement occurs for h = 5 nm and the enhancement factor $R_{PL} = I_{PL}^{(h = 5)}/I_{PL}^{(h = 100)}$ yields the largest value of 5.6, where $I_{PL}^{(h = 5)}$ and $I_{PL}^{(h = 100)}$ represents the PL intensity of CdS NW on the substrate with h of 5 and 100 nm, respectively. The PL enhancement factors are

dx.doi.org/10.1021/nl402836x | Nano Lett. 2013, 13, 5336−5343

3.3 and 1.7 for the h = 10 nm and h = 20 nm samples, respectively. Correspondingly, the TRPL decay transients are shown in Figure 5b. Generally, the PL decay rate (k_{PL}) is related to the radiative (k_R) and nonradiative (k_{NR}) recombination rates by: $k_{PL} = k_R + k_{NR}$.[40] We use the notations $k_{(100)}$ and $k_{(h)}$ to denote the total decay rates of the CdS excitons in the h = 100 nm sample and on those with thinner layer thicknesses of h = 5, 10, and 20 nm, respectively. From the PL decay profiles, we extract the decay rates as: $k_{(100)}$ = 0.62 ns^{-1}, $k_{(5)}$ = 2.5 ns^{-1}, $k_{(10)}$ = 1.6 ns^{-1} and $k_{(20)}$ = 0.96 ns^{-1}. The decay rates of $k_{(h)}$ are much larger than $k_{(100)}$ and with corresponding decay rate enhancement factor[54] $R_k = k_{(h)}/k_{(100)}$ at ~4.0; ~2.6; and ~1.5 for h = 5, 10, and 20 nm, respectively. The largest R_k value for h = 5 nm is attributed to the close proximity of the SPP in the Au film to the CdS NW excitons, giving rise to the strongest interactions.

The PL quantum yield quantitatively describes the emission efficiency of a system and is defined as $Q_{PL} = k_R/(k_R + k_{NR})$.[55] The quantum yield enhancement factor R_{QY}, can be deduced from the following two parameters: (a) the PL enhancement factor R_{PL} and (b) the decay rate enhancement factor R_K. The following two equations, $R_{PL} = R_{QY}|f(\lambda_{ex})|^2$ and $R_{QY} = (R_K)^{-1}|f(\lambda_{em})|^2$, express their relations, where $|f(\lambda_{ex})|$ and $|f(\lambda_{em})|$ are the local field enhancement factors at the excitation and emission wavelengths, respectively.[56,57] Combining the above two equations, the quantum yield enhancement obtained is $R_{QY} = |[f(\lambda_{em})]/[f(\lambda_{ex})]|(R_{PL}/R_K)^{1/2}$.[58] Given the proximity of the excitation and emission wavelengths to each other and the relatively flat plasmon resonance response from the Au film (see Supporting Information Figure S7), the absorption coefficients and the local field enhancement factors at the two wavelengths are rather similar.[59] Hence, we can approximate $|f(\lambda_{em})|/|f(\lambda_{ex})|^2 \approx \alpha(\lambda_{em})/\alpha(\lambda_{ex})$ and R_{QY} can be directly calculated using a simple relation $R_{QY} = |[\alpha(\lambda_{em})]/[\alpha(\lambda_{ex})]|^{1/2}(R_{PL}/R_K)^{1/2}$.[58] For a 60 nm thick Au film, the ratio of the absorption $\alpha(\lambda)$ at the emission and excitation wavelengths can be obtained from the absorption spectra over this range (see Supporting Information Figure S7). The quantum yield enhancement R_{QY} for the h = 5 nm sample was calculated to be 1.20 using the experimental inputs of R_{PL} =5.6 and R_K = 4.0. The R_{QY} are 1.13 and 1.06 for the h = 10 nm and h = 20 nm samples, respectively. The enhancement factors as a function of SiO_2 layer thickness h is summarized in Figure 5c. These findings strongly support the premise that the SPP coupling with excitons can drastically enhance the quantum efficiencies in CdS NWs through energy transfer from the SPPs in the Au film to the excitons in the CdS NWs, in agreement with many reported works.[55,60,61] These quantum efficiency enhancements also clearly show that there is no significant back energy transfer from the excitons in the CdS NW to the SPP in the Au films.

For dipoles near a metal−dielectric interface, the three processes involving the spectral overlap of SPP quanta for dipoles with SPP electric fields are (a) spontaneous emission of an SPP through the de-excitation of an excited dipole; (b) absorption of an SPP by a ground-state dipole to yield an excited state dipole; and (c) stimulated emission of an SPP clone through the de-excitation of an excited dipole.[19,62] From the enhanced quantum yield and the photonic properties, processes (a) and (c) should not play any significant role here. Hence, the mechanism for SPP-enhanced BM effect in our CdS NW devices is process (b). FDTD simulations in Figure 6 clearly shows that there is a strong local field between the CdS NWs and Au film for h = 5, 10, and 20 nm; while it is negligible for the h = 100 nm sample. Understandably, the strongest local field obtained from the simulations is for the sample with the thinnest SiO_2 layer. Given that the decay rate is affected by the strength of the local field in the SiO_2 layer, we can confidently conclude that the enhanced BM effect is a consequence of the strong coupling between the SPP and CdS excitons.

In summary, we demonstrated the lasing wavelength tuning of a single CdS NWs using the SPP-enhanced Burstein−Moss effect. We also proved that the BM effect is greatly enhanced in the hybrid metal/dielectric/semiconductor configuration as a consequence of the strong energy transfer from the SPP to the CdS excitons. Both the enhanced exciton emission intensities and recombination rates validate the presence of this strong interaction between the SPP and the excitons. The manipulation and application of their interactions at nanometer length scales could possibly lead to integrated nanophotonic laser sources that convert SPPs to photons or vice versa, permitting efficient coupling between plasmonic and photonic-based devices.

Methods. Au film with a thickness of 60 nm was prepared using a thermal evaporation method. Then SiO_2 layers with different thicknesses (5, 10, 20, and 100 nm) were deposited onto the Au film by magnetron sputtering. The surface morphology of the Au film before and after deposition of SiO_2 is measured by an atomic force microscope (AFM), see Supporting Information Figure S8. Highly crystalline CdS NWs were synthesized using a vapor transport method. The CdS NWs were deposited by spin-coating a suspension in ethanol onto the prepared Au films with varying SiO_2 thickness of 5, 10, 20, and 100 nm. The diameters of CdS NWs were determined by height measurements relative to the surface of substrate (AFM, Park Systems). The CdS NW lengths were determined from the scanning electron microscope (SEM, JEOL 7001F) images.

For lasing measurements, the laser source was a Coherent Legend regenerative amplifier (150 fs, 1 kHz, 800 nm) that was seeded by a Coherent Vitesse oscillator (120 fs, 80 MHz). The 800 nm wavelength laser pulses were from the regenerative amplifier's output while the 400 nm wavelength laser pulses were frequency doubled from the 800 nm fundamental with a BBO crystal. For steady-state PL and time-resolved PL measurement, the laser source was a Coherent Mira 900 (120 fs, 76 MHz) with the output laser pulse 800 nm and frequency doubled with a BBO crystal. For the single NW measurement, circularly polarized laser pulses generated using a 1/4 wave plate were focused onto an individual CdS NW using a Nikon microscope equipped with a 50× objective (NA = 0.45). This allows us to prevent the initial linearly polarized laser pulses from affecting our measurements. The PL emission signal from the NW was collected by the same microscope objective in a backscattering configuration and recorded by a cool-snap color camera to obtain the PL image. A 425 nm long pass filter was used to block the excitation laser. To obtain the PL spectra, the emission is collected by a Princeton Instrument spectrometer (PI Acton, Spectra Pro 2500i), dispersed by a grating of 600 g/mm and detected by a TE-cooled charge coupled detector camera (PIXIS-400B). For the TRPL measurements, the emission from a single NW was time-resolved by a streak camera system (Optoscope, Optronis GmbH) operating in the synchroscan mode with an ultimate temporal resolution of ~6 ps (at a scan speed of 100 ps/mm).

dx.doi.org/10.1021/nl402836x | Nano Lett. 2013, 13, 5336−5343

■ ASSOCIATED CONTENT

Supporting Information

TEM characterization, schematic of the experimental setup, emission spectra of CdS NWs with different diameters, lasing behavior of a single NW, lasing wavelength statistics of CdS NWs on different substrates, single CdS NW absorption, absorption spectra of Au film, and morphology characterization of Au films with and without SiO_2 coating. This material is available free of charge via the Internet at http://pubs.acs.org.

■ AUTHOR INFORMATION

Corresponding Authors

*E-mail: (T.C.S.) tzechien@ntu.edu.sg.
*E-mail: (Q.X.) qihua@ntu.edu.sg.

Author Contributions

‖X.L. and Q.Z. contributed equally to this work.

Notes

The authors declare no competing financial interest.

■ ACKNOWLEDGMENTS

T.C.S. acknowledges the support from the following research grants: NTU start-up Grant (M4080514); SPMS collaborative Research Award (M4080536); Ministry of Education (MOE) Academic Research Fund (AcRF) Tier 2 Grant MOE2011-T2-2-051. X.L. and T.C.S. also acknowledge the financial support by the Singapore National Research Foundation through the Competitive Research Programme under Project No. NRF-CRP5-2009-04 and the Singapore-Berkeley Research Initiative for Sustainable Energy (SinBerRISE) CREATE Programme. Q.X. acknowledges the support of this work from the Singapore National Research Foundation through a NRF fellowship Grant (NRF-RF2009-06) and a Competitive Research Program Grant (NRF-CRP-6-2010-2), Ministry of Education AcRF Tier 2 Grant (MOE2011-T2-2-051), and start-up Grant support (M58113004) from Nanyang Technological University (NTU).

■ REFERENCES

(1) Huang, M. H.; Mao, S.; Feick, H.; Yan, H. Q.; Wu, Y. Y.; Kind, H.; Weber, E.; Russo, R.; Yang, P. D. *Science* **2001**, *292* (5523), 1897–1899.
(2) Duan, X. F.; Huang, Y.; Agarwal, R.; Lieber, C. M. *Nature* **2003**, *421* (6920), 241–245.
(3) Zhang, Q.; Shan, X. Y.; Feng, X.; Wang, C. X.; Wang, Q. Q.; Jia, J. F.; Xue, Q. K. *Nano Lett.* **2011**, *11* (10), 4270–4274.
(4) Piccione, B.; Cho, C. H.; van Vugt, L. K.; Agarwal, R. *Nat. Nanotechnol.* **2012**, *7* (10), 640–645.
(5) Cho, C. H.; Aspetti, C. O.; Turk, M. E.; Kikkawa, J. M.; Nam, S. W.; Agarwal, R. *Nat. Mater.* **2011**, *10* (9), 669–675.
(6) Krogstrup, P.; Jorgensen, H. I.; Heiss, M.; Demichel, O.; Holm, J. V.; Aagesen, M.; Nygard, J.; Morral, A. F. I. *Nat. Photonics* **2013**, *7* (4), 306–310.
(7) Liu, X. F.; Zhang, Q.; Xiong, Q. H.; Sum, T. C. *Nano Lett.* **2013**, *13* (3), 1080–1085.
(8) Chu, S.; Wang, G. P.; Zhou, W. H.; Lin, Y. Q.; Chernyak, L.; Zhao, J. Z.; Kong, J. Y.; Li, L.; Ren, J. J.; Liu, J. L. *Nat. Nanotechnol.* **2011**, *6* (8), 506–510.
(9) Agarwal, R.; Barrelet, C. J.; Lieber, C. M. *Nano Lett.* **2005**, *5* (5), 917–920.
(10) Lieber, C. M. *MRS Bull.* **2003**, *28* (7), 486–491.
(11) Lu, Y. J.; Kim, J.; Chen, H. Y.; Wu, C. H.; Dabidian, N.; Sanders, C. E.; Wang, C. Y.; Lu, M. Y.; Li, B. H.; Qiu, X. G.; Chang, W. H.; Chen, L. J.; Shvets, G.; Shih, C. K.; Gwo, S. *Science* **2012**, *337* (6093), 450–453.
(12) Qian, F.; Li, Y.; Gradecak, S.; Wang, D. L.; Barrelet, C. J.; Lieber, C. M. *Nano Lett.* **2004**, *4* (10), 1975–1979.
(13) Liu, Y. K.; Zapien, J. A.; Shan, Y. Y.; Geng, C. Y.; Lee, C. S.; Lee, S. T. *Adv. Mater.* **2005**, *17* (11), 1372–1377.
(14) Pan, A. L.; Zhou, W. C.; Leong, E. S. P.; Liu, R. B.; Chin, A. H.; Zou, B. S.; Ning, C. Z. *Nano Lett.* **2009**, *9* (2), 784–788.
(15) Qian, F.; Gradecak, S.; Li, Y.; Wen, C. Y.; Lieber, C. M. *Nano Lett.* **2005**, *5* (11), 2287–2291.
(16) Li, J.; Meng, C.; Liu, Y.; Wu, X.; Lu, Y.; Ye, Y.; Dai, L.; Tong, L.; Liu, X.; Yang, Q. *Adv. Mater.* **2013**, *25* (6), 833–837.
(17) Fedyanin, D. Y.; Krasavin, A. V.; Arsenin, A. V.; Zayats, A. V. *Nano Lett.* **2012**, *12* (5), 2459–2463.
(18) Kena-Cohen, S.; Stavrinou, P. N.; Bradley, D. D. C.; Maier, S. A. *Nano Lett.* **2013**, *13* (3), 1323–1329.
(19) Berini, P.; De Leon, I. *Nat. Photonics* **2012**, *6* (1), 16–24.
(20) Liebermann, T.; Knoll, W. *Colloids Surf., A* **2000**, *171* (1–3), 115–130.
(21) García-Vidal, F. J.; Pendry, J. B. *Phys. Rev. Lett.* **1996**, *77* (6), 1163–1166.
(22) Park, I. Y.; Kim, S.; Choi, J.; Lee, D. H.; Kim, Y. J.; Kling, M. F.; Stockman, M. I.; Kim, S. W. *Nat. Photonics* **2011**, *5* (11), 678–682.
(23) Wurtz, G. A.; Pollard, R.; Zayats, A. V. *Phys. Rev. Lett.* **2006**, *97*, 5.
(24) Ebbesen, T. W.; Lezec, H. J.; Ghaemi, H. F.; Thio, T.; Wolff, P. A. *Nature* **1998**, *391* (6668), 667–669.
(25) De Leon, I.; Berini, P. *Nat. Photonics* **2010**, *4* (6), 382–387.
(26) Ma, R. M.; Oulton, R. F.; Sorger, V. J.; Bartal, G.; Zhang, X. A. *Nat. Mater.* **2011**, *10* (2), 110–113.
(27) Sorger, V. J.; Pholchai, N.; Cubukcu, E.; Oulton, R. F.; Kolchin, P.; Borschel, C.; Gnauck, M.; Ronning, C.; Zhang, X. *Nano Lett.* **2011**, *11* (11), 4907–4911.
(28) Russell, K. J.; Liu, T.-L.; Cui, S.; Hu, E. L. *Nat. Photonics* **2012**, *6* (7), 459–462.
(29) Burstein, E. *Phys. Rev.* **1954**, *93* (3), 632–633.
(30) Moss, T. S. *Proc. Phys. Soc. B* **1954**, *67*, 775.
(31) Banyai, L.; Koch, S. W. *Phys. Rev. Lett.* **1986**, *57* (21), 2722–2724.
(32) Yang, Y. H.; Chen, X. Y.; Feng, Y.; Yang, G. W. *Nano Lett.* **2007**, *7* (12), 3879–3883.
(33) Sun, Q. C.; Yadgarov, L.; Rosentsveig, R.; Seifert, G.; Tenne, R.; Musfeldt, J. L. *ACS Nano* **2013**, *7* (4), 3506–3511.
(34) Grundmann, M. *The Physics of Semiconductors, An Introduction including Devices and Nanophysics*; Springer: New York, 2006.
(35) Barnes, W. L.; Dereux, A.; Ebbesen, T. W. *Nature* **2003**, *424* (6950), 824–830.
(36) Ebbesen, T. W.; Genet, C.; Bozhevolnyi, S. I. *Phys. Today* **2008**, *61* (5), 44–50.
(37) Liu, X.; Zhang, Q.; Xing, G.; Xiong, Q.; Sum, T. C. *J. Phys. Chem. C* **2013**, *117* (20), 10716–10722.
(38) Liu, X. F.; Wang, R.; Jiang, Y. P.; Zhang, Q.; Shan, X. Y.; Qiu, X. H. *J. Appl. Phys.* **2010**, *108* (5), 054310–054313.
(39) Li, D.; Zhang, J.; Xiong, Q. H. *ACS Nano* **2012**, *6* (6), 5283–5290.
(40) Okamoto, K.; Vyawahare, S.; Scherer, A. *J. Opt. Soc. Am. B* **2006**, *23* (8), 1674–1678.
(41) Oulton, R. F.; Sorger, V. J.; Zentgraf, T.; Ma, R. M.; Gladden, C.; Dai, L.; Bartal, G.; Zhang, X. *Nature* **2009**, *461* (7264), 629–632.
(42) Johnson, J. C.; Yan, H.; Yang, P.; Saykally, R. J. *J. Phys. Chem. B* **2003**, *107* (34), 8816–8828.
(43) Johnson, P. B.; Christy, R. W. *Phys. Rev. B* **1972**, *6* (12), 4370–4379.
(44) Puthussery, J.; Lan, A.; Kosel, T. H.; Kuno, M. *ACS Nano* **2008**, *2* (2), 357–367.
(45) Duan, X.; Huang, Y.; Agarwal, R.; Lieber, C. M. *Nature* **2003**, *421* (6920), 241–245.
(46) Pauzauskie, P. J.; Yang, P. *Mater. Today* **2006**, *9* (10), 36–45.
(47) Sharma, S. N.; Pillai, Z. S.; Kamat, P. V. *J. Phys. Chem. B* **2003**, *107* (37), 10088–10093.

(48) Subramanian, V.; Wolf, E. E.; Kamat, P. V. *J. Phys. Chem. B* **2003**, *107* (30), 7479−7485.
(49) Ardo, S.; Sun, Y.; Staniszewski, A.; Castellano, F. N.; Meyer, G. J. *J. Am. Chem. Soc.* **2010**, *132* (19), 6696−6709.
(50) Verdenhalven, E.; Binder, R.; Knorr, A.; Malić, E. *Chem. Phys.* **2013**, *413* (0), 3−10.
(51) Titova, L. V.; Hoang, T. B.; Jackson, H. E.; Smith, L. M. *Appl. Phys. Lett.* **2006**, *89* (5), 053119−053111.
(52) Versteegh, M. A. M.; Vanmaekelbergh, D.; Dijkhuis, J. I. *Phys. Rev. Lett.* **2012**, *108* (15), 157402.
(53) Soci, C.; Zhang, A.; Bao, X. Y.; Kim, H.; Lo, Y.; Wang, D. L. *J. Nanosci. Nanotechnol.* **2010**, *10* (3), 1430−1449.
(54) Purcell, E. M. *Phys. Rev.* **1946**, *69* (11−1), 681−681.
(55) Okamoto, K.; Niki, I.; Shvartser, A.; Narukawa, Y.; Mukai, T.; Scherer, A. *Nat. Mater.* **2004**, *3* (9), 601−605.
(56) Bardhan, R.; Grady, N. K.; Cole, J. R.; Joshi, A.; Halas, N. J. *ACS Nano* **2009**, *3* (3), 744−752.
(57) Govorov, A. O.; Bryant, G. W.; Zhang, W.; Skeini, T.; Lee, J.; Kotov, N. A.; Slocik, J. M.; Naik, R. R. *Nano Lett.* **2006**, *6* (5), 984−994.
(58) Wang, Y.-L.; Nan, F.; Liu, X.-L.; Zhou, L.; Peng, X.-N.; Zhou, Z.-K.; Yu, Y.; Hao, Z.-H.; Wu, Y.; Zhang, W.; Wang, Q.-Q.; Zhang, Z. *Sci. Rep.* **2013**, *3*, 1861.
(59) Kulakovich, O.; Strekal, N.; Yaroshevich, A.; Maskevich, S.; Gaponenko, S.; Nabiev, I.; Woggon, U.; Artemyev, M. *Nano Lett.* **2002**, *2* (12), 1449−1452.
(60) Pacifici, D.; Lezec, H. J.; Atwater, H. A. *Nat. Photonics* **2007**, *1* (7), 402−406.
(61) Heidel, T. D.; Mapel, J. K.; Singh, M.; Celebi, K.; Baldo, M. A. *Appl. Phys. Lett.* **2007**, *91* (9), 093506−093508.
(62) Ding, K.; Ning, C. Z. *Light Sci Appl.* **2012**, *1*, e20.

dx.doi.org/10.1021/nl402836x | *Nano Lett.* 2013, 13, 5336−5343

Supporting Information for

Wavelength Tunable Single Nanowire Lasers Based on Surface Plasmon Polariton Enhanced Burstein-Moss Effect

Xinfeng Liu,[1†] Qing Zhang,[1†] Jing Ngei Yip,[1] Qihua Xiong,[1,2,#] Tze Chien Sum[1,3,*]

[1]Division of Physics and Applied Physics, School of Physical and Mathematical Sciences, Nanyang Technological University, Singapore 637371

[2]NOVITAS, Nanoelectronics Center of Excellence, School of Electrical and Electronic Engineering, Nanyang Technological University, Singapore 639798

[3]Energy Research Institute @ NTU (ERI@N), Nanyang Technological University, 50 Nanyang Drive, Singapore 637553

[†] These authors contribute equally to this work.

To whom correspondence should be addressed, *Email: tzechien@ntu.edu.sg and [#]Email:qihua@ntu.edu.sg

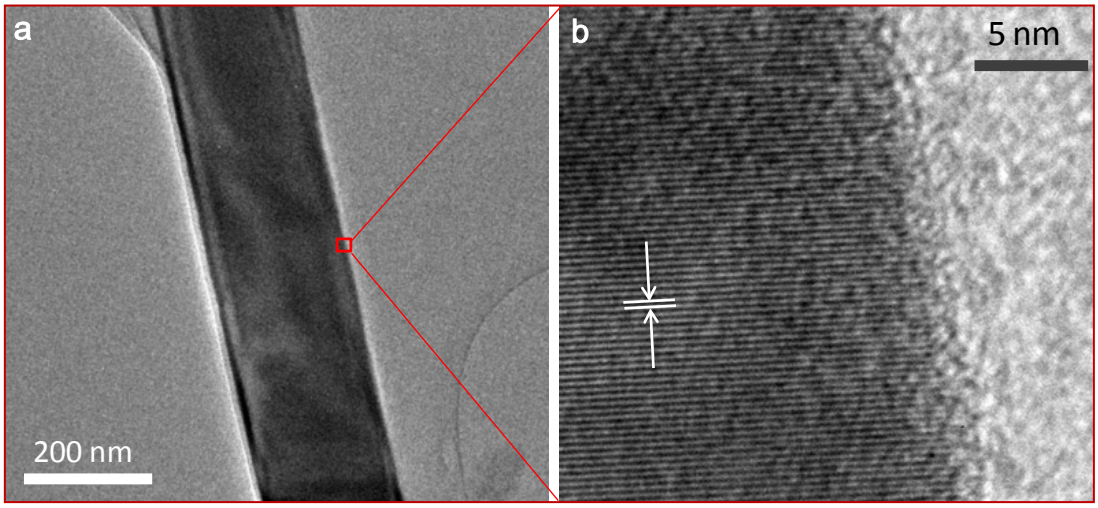

Figure S1 TEM image (a) and HRTEM pattern (b) of a typical CdS NW.

The as-grown CdS nanowires have a single crystalline lattice structure with a lattice spacing of h_{CdS} ~0.33 nm along the [002] lattice plane corresponding to a wurzite crystal lattice (Figure S1).

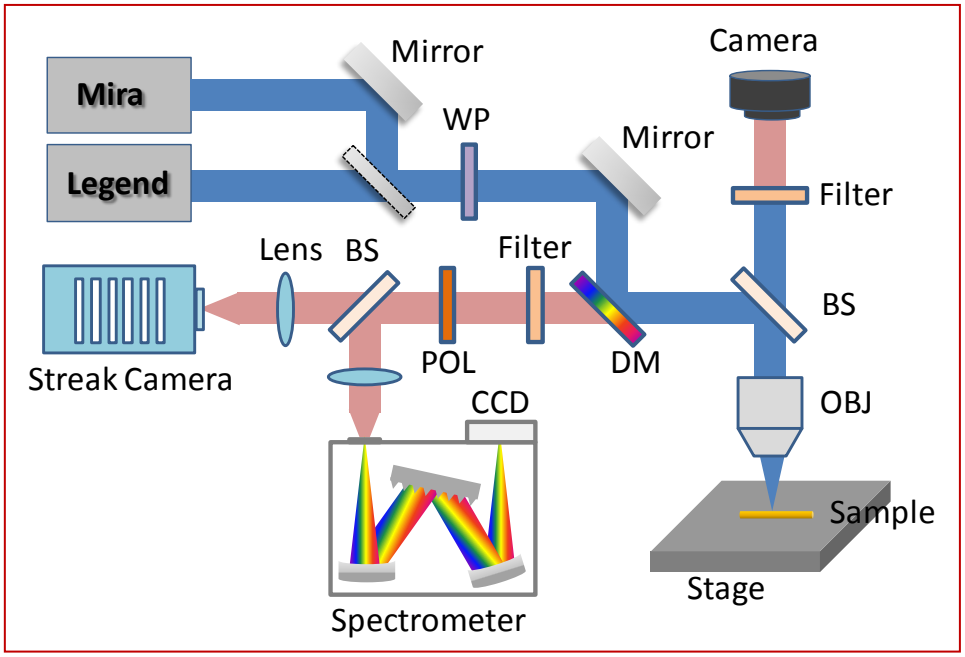

Figure S2 A schematic of the home-built confocal microscope setup for measuring the optical properties of single CdS NWs. WP: Wave Plate; BS: Beam Splitter; DM: Dichroic Mirror; POL: Polarizer; OBJ: Objective.

For lasing measurements, the laser source used was a Coherent Legend regenerative amplifier (150 fs, 1 kHz, 800 nm) that was seeded by a Coherent Vitesse oscillator (100 fs, 80 MHz). The 800 nm wavelength laser pulses were from the regenerative amplifier's output while the 400 nm wavelength laser pulses were frequency doubled from the 800 nm fundamental with a BBO crystal. For steady-state photoluminescence (PL) and time-resolved PL measurement, the laser source was a Coherent Mira 900 (120 fs, 76 MHz) with the output laser pulse 800 nm and frequency doubled with a BBO crystal. For the single NW measurement, the linearly polarized laser pulses were converted to circularly polarized pulses using a 1/4 wave plate to eliminate the effect of pump laser polarization on the measurements. These pulses were focused onto an individual CdS NW using a home-built confocal microscope equipped with a 50× objective (NA = 0.45). The PL emission signal from the NW was collected by the same microscope objective in a backscattering configuration and recorded by a cool-snap color camera to obtain the PL image. A 425 nm long pass filter was used to block the excitation laser. To obtain the PL spectra, the collected emission is collected by a Princeton Instrument spectrometer (PI Acton, Spectra Pro 2500i), dispersed by a

grating of 600 g/mm and detected by a TE-cooled charge coupled detector camera (PIXIS-400B). Images shown in Figure S4 were obtained with the same system by replacing the grating with a mirror. For the TRPL measurements, the emission from a single NW was time-resolved by a streak camera system (Optoscope^{TM}, Optronis GmbH) operating in the synchroscan mode with an ultimate temporal resolution of ~6 ps (at a scan speed of 100ps/mm).

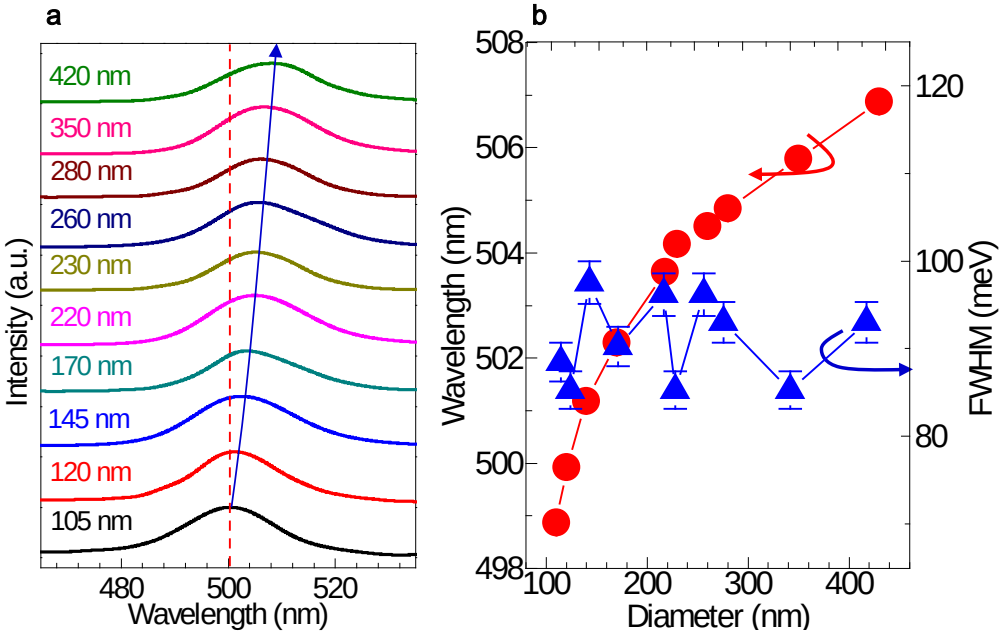

Figure S3 (a) The emission spectra of CdS NWs with different diameters, the pump power was fixed at 0.1 μJ/cm^2. (b) The diameter-dependent emission peak energy and full width at half maximum (FWHM).

The emission spectra of single CdS nanowires with different diameters are measured at room temperature with a 400 nm excitation wavelength at a fixed pump power of 0.1μJ/cm^2. The spectra are shown in Figure S3 (a). Only one peak is observed at around 500 nm, which is attributed to the band-edge emission (BE) of CdS. With increasing CdS NW diameters, the emission peak positions are red-shifted. The emission peak positions and the FWHM are plotted in Figure S3 (b). The dependence of the emission peak and lasing wavelength on the NW length can be found in Reference 1.

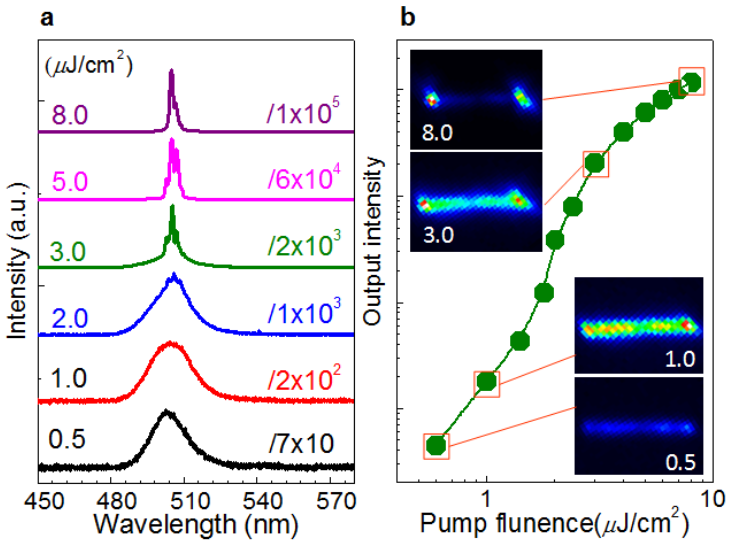

Figure S4 (a) Emission spectra for a ~10 μm long CdS NW with diameter ~220 nm – photo-excited with different pump fluences (0.5 to 8.0μJ/cm^2). (b) A plot of the integrated PL intensity as a function of pump fluence, illustrating the occurrence of lasing. These experiment data are fitted using a multi-mode lasing model [Reference 2-6] and the threshold is ~2μJ/cm^2. Insets are several representative CCD images of the CdS NW emission.

For calibration and comparison, we measured the emission spectra of NW laser devices on a substrate with a SiO_2 thickness of h ~100 nm. The CdS NWs were spin-coated on this SiO_2/Au/Si substrate. In this case, the penetration depth ($Z = \lambda / 2\pi[(\varepsilon'_{SiO2} - \varepsilon'_{Au}) / \varepsilon'^{2}_{Au}]^{1/2}$, where ε'_{SiO_2} and ε'_{Au} are the real parts of the dielectric constants of SiO_2 and Au) of surface plasmon fringing into the semiconductor is calculated to be ~77 nm. Hence, for a 100 nm thick layer, the SPP effect is expected to be negligible – consistent with the reported results for typical bare NW lasers. The room-temperature lasing characteristics of a hybrid device (CdS NW diameter ~220 ± 10 nm, length ~10 ± 0.5 μm, h ~100 nm) were measured as a function of pump fluence (0.5 to 8.0μJ/cm^2). Figure S4a clearly illustrates the transition from spontaneous emission to lasing action. It should be noted that the lasing wavelength merely shifts ~2 nm with increasing the pump fluence – verifying that the BM shift is indeed relatively weak in the undoped CdS NWs (and in the absence of any SPP coupling).

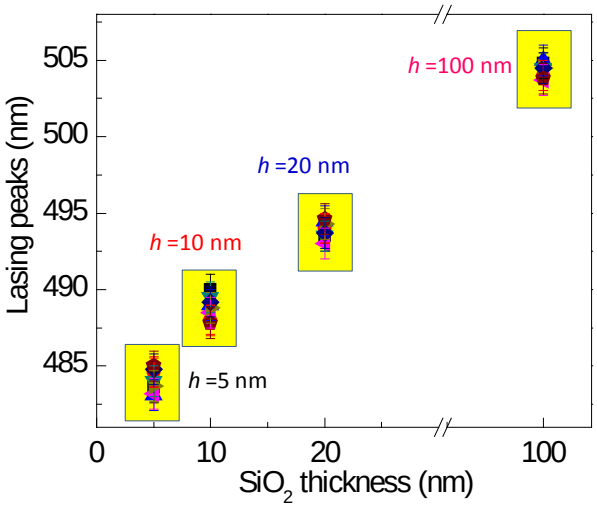

Figure S5 The lasing peak positions of four groups of CdS NWS on substrates with different thickness (*h*) of SiO_2. Each group comprises of 8 different NWs of comparable dimensions. The pump fluence was fixed at ~8μJ/cm^2.

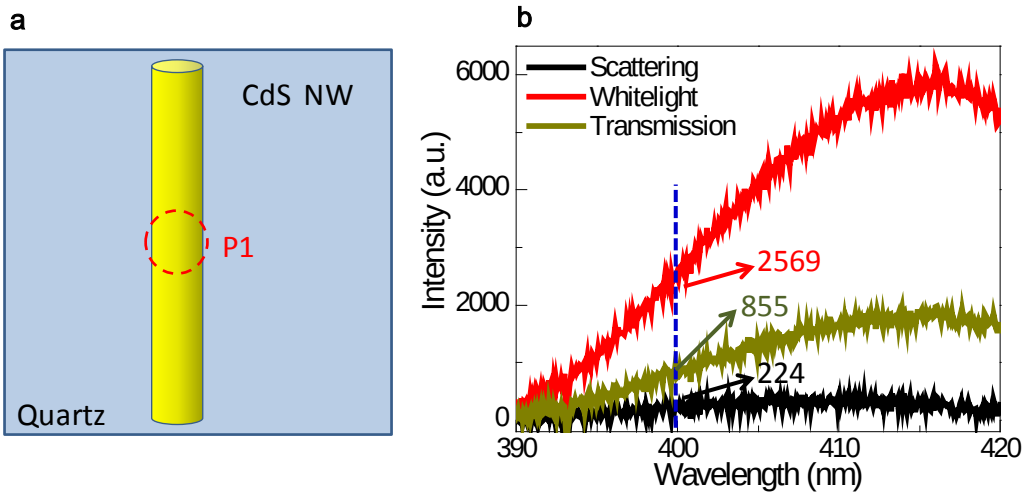

Figure S6 (a) A schematic of the measurements to determine the amount of absorption from a single 100 nm diameter CdS NW. Using a confocal microscope, we measured the transmission and scattering spectra separately and then used them to calculate the amount of light absorption from a single NW. The red circle is the focal area. (b) The corresponding scattering, transmission and white light spectra measured at P1. The dashed blue line represents the wavelength of excitation laser at 400 nm. The intensities of the scattering, transmission and white light are 224, 855 and 2569, respectively (arbitrary units).

From the scattering, transmission and white light spectra measured at P1, we can estimate the amount of absorption from a single CdS NW at 400 nm. The percentage of the incident light absorbed is calculated as follows: [(2569-855)/2569－224/2569] = 57%.

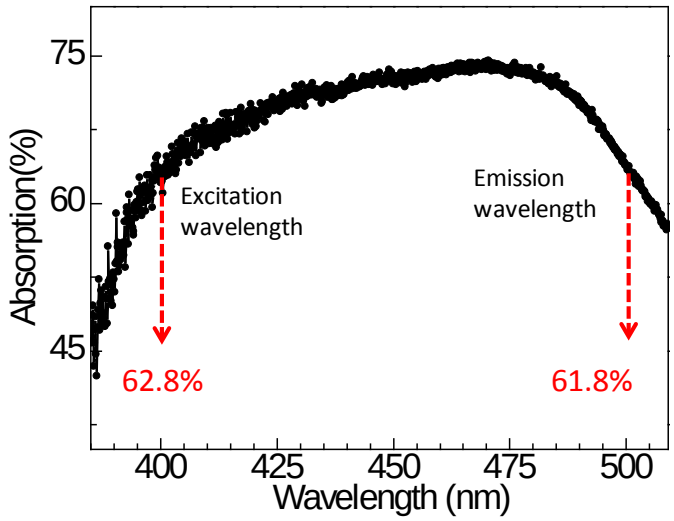

Figure S7 The absorption spectrum measured on a 60 nm thick Au film over the range from 380 nm to 510 nm. This spectrum was measured to determine the % absorption at the excitation wavelength (~400 nm) and emission wavelength (~500 nm).

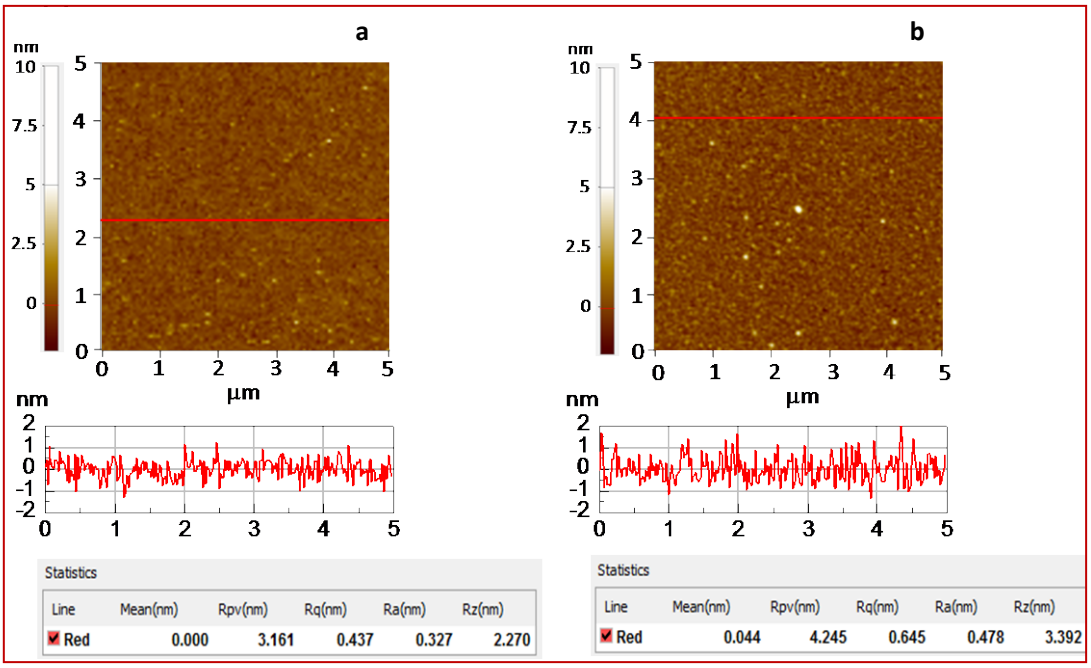

Figure S8 AFM images, line scan and the statistical values of the surface roughness of Au film before (a) and after (b) deposition of a SiO_2 layer.

For the Au film of thickness ~60 nm, the average surface roughness is around 0.3 nm (over a scan area of $5 \times 5\ \mu m^2$), as shown in Figure S8 (a), suggesting that the Au film is very flat. After SiO_2 layer deposition, the surface roughness increased to around 0.5 nm (see Figure S8 b).

References:

1. X. F Liu, Q Zhang, Q. H. Xiong, T. C. Sum, Nano Letters 2013, **13** (3), 1080-1085.
2. L. W. Casperson, M. Khoshnevissan, Journal of Applied Physics 1994, **75** (2), 737-747.
3. Mariano A. Zimmler, Jiming Bao, Federico Capasso, Sven Müller, and Carsten Ronning, Appl. Phys. Lett. 2008, **93**, 051101.
4. Fang Qian, Yat Li, Silvijia Gradecak, Hong Gyu Park, Yajie Dong, ZhongLin Wang, and Charles M. Lieber, Nature Materials, 2008, **7**,701.
5. Geburt S, Thielmann A, Roder R, Boder R, Borschel C, McDonnell A, Kozlik M, Kuhnel J, Sunter KA, Capasso F, Ronning C, 2012, **23**, 365204.
6.S. Chu, G. P. Wang, W. H. Zhou, Y. Q. Lin, C. Leonid, J. Z. Zhao, J. Y. Kong, L. Lin, J. J. Ren, J. L. Liu, Nature nanotechnology, 2011, **6**, 506.